Peer-reviewed version available at Nanomaterials 2019, 9, 968; doi:10.3390/nano9070968

Article

Toxicity of TiO_2, ZnO and SiO_2 nanoparticles in human lung cells: Safe-by-design development of construction materials

Monika Remzova[1], Radek Zouzelka[1], Tana Brzicova[2], Kristyna Vrbova[2], Dominik Pinkas[3], Pavel Rőssner[2], Jan Topinka[2] and Jiri Rathousky[1,*]

[1] J. Heyrovsky Institute of Physical Chemistry of the CAS, Dolejskova 3, Prague 18223, Czech Republic; monika.remzova@jh-inst.cas.cz, radek.zouzelka@jh-inst.cas.cz, jiri.rathousky@jh-inst.cas.cz
[2] Institute of Experimental Medicine of the CAS, Videnska 1083, Prague 14220, Czech Republic; tana.brzicova@iem.cas.cz, krystina.vrbova@iem.cas.cz, pavel.rossner@iem.cas.cz, jan.topinka@iem.cas.cz
[3] Institute of Molecular Genetics of the CAS, Microscopy Center, Electron Microscopy Core Facility, Prague 14220, Czech Republic; dominik.pinkas@img.cas.cz
* Correspondence: jiri.rathousky@jh-inst.cas.cz; Tel.: +4202 6605 3945

Abstract: Rapid progress in the development of highly efficient nanoparticle-based construction technologies has not always been accompanied by a corresponding understanding of their effects on human health and ecosystems. Here, we compare toxicological effects of pristine TiO_2, ZnO and SiO_2, and coated SiO_2 nanoparticles and evaluate their suitability as additives to consolidants of weathered construction materials. First, WST-1 and LDH assays were used to determine the viability of human alveolar A549 cells at various nanoparticle concentrations (0–250 μg mL^{-1}). While the pristine TiO_2 and coated SiO_2 nanoparticles did not exhibit any cytotoxic effect up to the highest tested concentration, the pristine SiO_2 and ZnO nanoparticles significantly reduced cell viability. Second, as all the developed nanoparticle-modified consolidants increased the mechanical strength of weathered sandstone, the decisive criterion for the selection of the most suitable nanoparticle additive was as low toxicity as possible. We believe that this approach will be of high importance for industry to identify materials representing top functional properties and low toxicity at an early stage of the product development.

Keywords: SiO_2 nanoparticles; ZnO nanoparticles; TiO_2 nanoparticles; toxicity; ethylsilicate consolidants

1. Introduction

Nanoparticles are widely used because they can improve both quantitative and qualitative properties of technological materials [1]. In the construction industry, they can enhance mechanical properties of the materials used to consolidate weathered building materials [2]. However, their production, handling and use can pose health and environmental risks that potentially limits their benefits.

From the application point of view, SiO_2, ZnO and TiO_2 form a triad of the most commonly used oxide nanoparticles. While their surface properties are comparable, their structure properties differ substantially, particularly their solubility and conductivity. While TiO_2 is an insoluble ceramic and SiO_2 practically insoluble, ZnO displays considerable solubility in weak acids and thus suffers from photocorrosion [3]. ZnO and TiO_2 are semiconductors with a similar band-gap [4–7] whereas SiO_2 is an insulant.

However, these properties are associated with a broad range of toxicological effects. In terms of solubility, practically insoluble SiO_2 nanoparticles have been shown to induce reactive oxygen species (ROS) autophagy in human hepatocytes [8], spermatogenesis damage [9] and impairment of vascular homeostasis [10]. Soluble ZnO nanoparticles release toxic zinc ions, before or after their uptake into cells; their toxic effects exhibit a sharp concentration dependence indicating the presence of a critical Zn^{2+} ion concentration [11]. Overtreatment with zinc ions causes a cell to lose its control functions and commit apoptosis [12]. In terms of semiconductivity, the toxicity of zinc oxide nanoparticles can be increased by the photocatalytic effect [13] In the case of insoluble TiO_2 semiconductor nanoparticles, they do not appear to become toxic under dark or non-UV exposure conditions [14], but toxicity has been reported after UV exposure [15].

From the above, it should be obvious that when developing any nanoparticle-based technology, the toxicological impact of nanoparticles needs to be taken into account [16]. However, this aspect is generally neglected, with nanoparticles often selected only on the basis of their function. Consequently, in many cases, the developed technologies are not safe-by-design.

Therefore, in this study, we developed safe-by-design highly efficient consolidants for weathered construction materials. First, we assessed the cytotoxicity of five types of oxide nanoparticles (TiO_2, ZnO and SiO_2, and octyl- and methyl-modified SiO_2). Second, based on results of two different cytotoxicity tests, we formulated nanoparticle-modified consolidants with optimized composition to achieve high performance characteristics with minimum health hazard. Our research shows that the often-used toxic nanoparticles can be replaced by non-toxic equivalents without any performance impairment.

2. Materials and Methods

2.1. Nanoparticles and their characterization

Five commercially available metal oxide nanoparticles were tested, including

Aeroxide® TiO_2 P25 (Evonik Industries, Germany); Aerosil® SiO_2 200 Pharma, R805, R9200 (Evonik Industries, Germany) and NanoZnO (Bochemie, Czech Republic).

Aerosil® SiO_2 A200 (hereinafter referred to as SiO_2) is a nanopowder with a surface area of 220 $m^2\ g^{-1}$ and particle size of 12 nm (both according to the manufacturer).

Aerosil® R9200 (hereinafter referred to as SiO_2–methyl) is a nanopowder of SiO_2 with a methylated surface, its surface area and particle size being 150–190 $m^2\ g^{-1}$ and 12 nm (both according to the manufacturer), respectively.

Aerosil®R805 (hereinafter referred to as SiO_2–octyl) is a nanopowder of SiO_2 with an octylated surface, its surface area and particle size being 125–175 $m^2\ g^{-1}$ and 12 nm (both according to the manufacturer), respectively.

Aeroxide® TiO_2 P25 (hereinafter referred to as TiO_2) is a photocatalyst widely used owing to its high activity in many photocatalytic reactions. It contain more than 70% of anatase phase with a minor proportion of rutile (about 20%) and a small percentage of amorphous phase [17]. It exhibits a specific surface area in the range of 35–65 $m^2\ g^{-1}$ and a particle size of 25 nm (according to the manufacturer).

NanoZnO (hereinafter referred to as ZnO) is a photocatalyst with a surface area and particle size of 90–110 $m^2\ g^{-1}$ and 17 nm (both according to the manufacturer), respectively.

The morphological properties of the nanoparticles were determined by the analysis of adsorption isotherms of nitrogen or krypton at ca 77 K using a Micrometrics 3Flex volumetric adsorption unit and by scanning electron microscopy (Joel JSM-6700F microscope). The size distribution and zeta potential of the nanoparticles in dispersions (in water-bovine serum albumin (BSA) and cell culture medium) was measured by dynamic light scattering using ZetaSizer Nano ZS (Malvern Instruments Ltd., Malvern, UK). The structure properties of the nanoparticles were determined by FTIR spectroscopy using a Nicolet 6700 apparatus.

2.2. Preparation of the nanoparticle dispersions for cytotoxicity testing

To dispersed hydrophobic nanoparticles in water-based systems, first, they were treatment with ethanol (70 %). Afterwards, the nanoparticles were dispersed in deionized water (2.56 mg mL^{-1}) containing 0.05% BSA and sonicated by probe at 400 W with amplitude of 10% (Digital Sonifier S-450d equipped with a standard 13-mm disruptor horn, Branson, USA) for 16 minutes in an ice bath. Before exposure to the cells, the nanoparticle dispersions were gradually diluted in the cell culture medium containing 1% fetal bovine serum (FBS) to their final concentration ranged from 1 to 250 μg mL^{-1}.

2.3. Cell cultivation and exposure to the nanoparticles

The A549 cell line (human type II pulmonary epithelial cells, CCL-185™ ATCC) was cultured in minimal essential medium (MEM) + Glutamax (Gibco™, Thermo Fisher Scientific) and FBS of 10% (v/v) (Gibco™, Sigma-Aldrich) in an incubator (37 °C, 5 % CO_2). For the cytotoxicity testing, the cells were seeded overnight in 96-well microtiter plates with 7500 cells per well and incubated overnight. Freshly prepared nanoparticles at the above given concentrations were added to the wells and incubated for 24 h (37 °C, 5 % CO_2)

2.4. Cytotoxicity testing

WST-1 assay: After the exposure period, the cell culture medium was removed and the cells were rinsed twice with Phosphate Buffered Saline (PBS). The Cell Proliferation Reagent WST-1 (Roche Diagnostics) and a phenol red free MEM containing 1% PBS was mixed in a ratio of 1:10. Afterwards, 120 μl of this mixture was added to each test well and incubated at 37 °C for 1 hour. To prevent interference of nanoparticles adsorbed on the plate plastic with absorbance reading, 100 μL of supernatants from each well were transferred to a new plate. The absorbance of the well content was measured at the wavelength of 450 nm using a SpectraMax® M5 Plate Reader (Molecular Device). To determine the cell viability, the background absorbance of the well content without cells was subtracted. The viability of the nanoparticle treated lung cells was expressed as a ratio of the sample absorbance (Abs sample) and that of average negative control (100 % viable, designated as average Abs NC)

$$\% \text{ viability} = (\text{Abs sample} / \text{average Abs NC}) \times 100 \quad (1)$$

As Zn^{2+} ions can be released from the ZnO nanoparticles, we employed the WST-1 assay with ZnCl2 to determine their cytotoxicity effect. The exposure concentrations were adjusted to provide the same dose of elemental Zn.

LDH assay: After 24 h incubation, 50 μL supernatant from each well was used to determine the released LDH activity ($LDH_{supernatants}$).

The viable cells were washed with PBS and incubated with 100 μL of a Triton X-100 solution in cell culture medium (1 % wt., Sigma-Aldrich) at 37 °C for 30 min. 50 μL of the supernatant from each well was used for the measurement of the LDH activity of viable cells ($LDH_{lysates}$).

50 μL of the reaction mixture of the Cytotoxicity Detection Kit (LDH) (Roche Diagnostics) was added to both above prepared supernatants and incubated in the dark for 15 min. Finally, 25 μL of 10 nM HCl was added to each well to terminate the reaction and the absorbance at 490 nm was measured using the SpectraMax® M5 Plate Reader. To determine the viability, the background absorbance of the well content without cells was subtracted. The cell viability was calculated according to the following formula

$$\% \text{ viability} = (LDH_{lysates} / LDH_{lysates} + LDH_{supernatants}) \times 100 \quad (2)$$

2.5. Data analysis and statistics

The toxicity experiments were done in three replicates for all treatments. Significant differences between compared samples were determined by using Student's t test where p values were used as

Peer-reviewed version available at Nanomaterials 2019, 9, 968; doi:10.3390/nano9070968

the threshold for statistical significance. An analysis of variance (ANOVA) followed by a Dunnett's test was performed (The Prism 5 program, GraphPad Software, San Diego, CA, USA). The data are expressed as a mean ± a standard deviation (SD). LC_{50} values (concentrations that inhibited cell viability by 50 %) were calculated using four-parameter log-logistic models in the drc package in the statistical software R (version 3.4.0.) [18].

2.6. Nanoparticle uptake by the cells determined by transmission electron microscopy

The cultivation of the cells in the presence of the nanoparticle dispersion (10 μg ml^{-1}) on glass coverslips of 12 mm (Schott Glass AG) was carried out in the wells of a 24-well plate. After 24 h exposure, first, the cells were washed with Sörensen buffer (0.1 M sodium/potassium phosphate buffer, pH 7.3; designated as SB), then treated with a 2.5 % glutaraldehyde solution in SB for 2 h, afterwards washed with SB, and, finally, treated with a 1 % OsO4 solution in SB for 2 h. Subsequently, the cells were dehydrated in acetone and embedded in Epon-Durcupan resin, which polymerized within 72 h at 60 °C. Ultrathin sections (80 nm) were placed on 200 mesh size copper grids and stained with uranyl acetate and lead citrate. The visualization was performed using a FEI Morgagni 268 transmission electron microscope operated at 80 kV equipped with a Mega View III CCD camera (Olympus Soft Imaging Solutions).

2.7. Preparation of the nanoparticle-modified consolidants

The consolidants were prepared by adding the nanoparticles (3 % wt.) (see above) to Dynasylan®40 (Evonik), which is an ethylsilicate oligomer. Afterwards, catalyst n-octylamine (0.18 % wt.) (Alfa Aesar) was added. The mixture obtained was diluted with isopropanol in the ratio 1:1. For the consolidant containing ZnO nanoparticles, a mixture of n-octylamine and dibutyltin dilaurate (DBTL) was used because n-octylamine was not sufficient to achieve a formation of the gel. An overview of the consolidants is given in the Table 1. Here SiGel designates the consolidant containing Dynasylan®40, catalyst and given nanoparticles. The commercial consolidant KSE OH (Remmers) was used as reference. Compared to our developed consolidants, KSE OH contains only 25 % of solvents, while ours 50 %. According to the data sheet, this product should be suitable for the consolidation of weathered, friable natural stones, particularly sandstones, cast stone, renders and mortar.

Table 1. An overview of the consolidants for the weathered sandstone.

Consolidant	Catalyst
KSE OH (commercial reference)	dibutyltin dilaurate
SiGel SiO_2	n-octylamine
SiGel SiO_2-methyl	n-octylamine
SiGel SiO_2-octyl	n-octylamine
SiGel TiO_2	n-octylamine
SiGel ZnO	n-octylamine + dibutyltin dilaurate

2.8. Evaluation of the consolidation effect

The naturally weathered sandstone (Prosek Rocks, Prague, Czech Republic) of high porosity and low strength was selected as a material modelling highly weathered construction material. This sandstone is an ocher colored fine-grained clastic sedimentary rock, its mineral composition consisting of 93 % of quartz clasts and of 7 % of clay matrix (kaolinite, often impregnated with iron-oxyhydroxides). Blocks of the sandstone 3 × 3 × 3 cm in size were impregnated with the consolidants by capillary soaking until the complete filling of the sandstone porous system. After six months, the mechanical properties of the treated stones were determined using a drilling resistance measuring system (DRMS) (SINT Technology). Drill bits of 4.8 mm diameter at a rotation speed of 300 rpm and a penetration rate of 30 mm/min were used.

3. Results and Discussion

3.1. Physico-chemical properties of nanoparticles

For the nanoparticles in powder form, nanoparticle aggregation was observed (Figure 1). The SiO_2 nanoparticles formed large fluffy highly porous aggregates while those of the coated were smaller, especially those of methylated ones. The aggregates of the TiO_2 nanoparticles were much smaller and rather inhomogeneous. Compared to the spherical character of the above-mentioned nanoparticles, the ZnO nanoparticles exhibited rather different shape of platelets, which is clearly due to their crystallinity. The insets in Figure 1 show details of the particle structure and morphology. While amorphous SiO_2 nanoparticles, both uncoated and coated, exhibit characteristic spherical shape, highly crystalline TiO_2 and ZnO nanoparticles differ in their morphology, being prismatic and platelet one, respectively. The size of the uncoated and coated SiO_2 and TiO_2 nanoparticles was comparable of 15-20 nm. However, compared to SiO_2 nanoparticles the ZnO ones were smaller of about 10 nm and more aggregated.

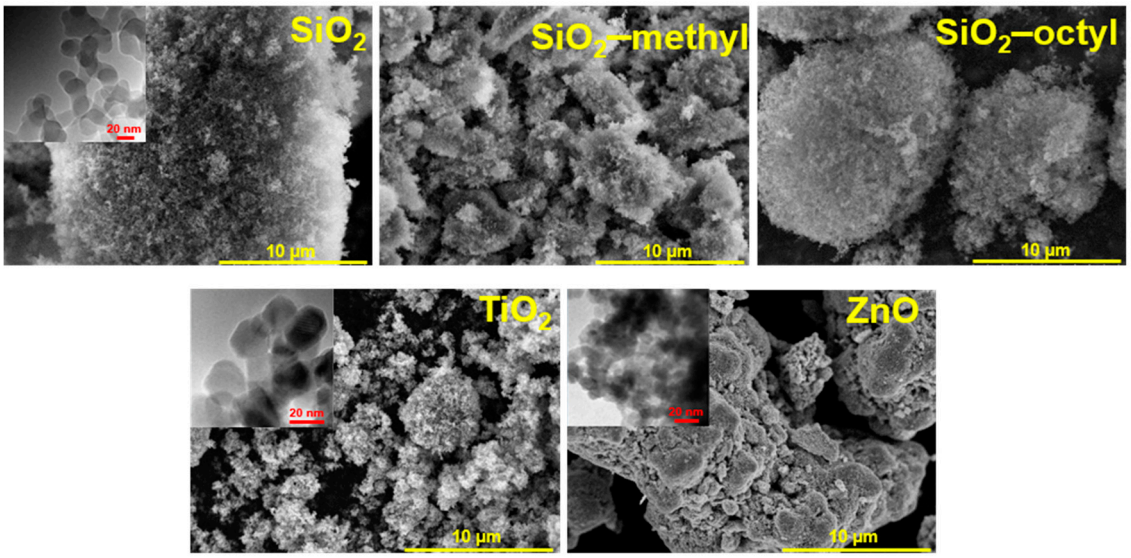

Figure 1. SEM images of the tested nanoparticles used for toxicological testing. The insets show details of particles morphology determined by HRTEM.

The size of the primary particles calculated from the BET surface area, provided the crystals were approximated by a sphere, was in agreement with those determined from HRTEM images (Table 2, Figure 1). For SiO_2 nanoparticles, the calculated primary size was in the range as that determined from HRTEM because the aggregates were very loose with complete accessibility of the surface. However, for TiO_2 and ZnO the calculated values overestimate the particle size obtained by HRTEM because these particles formed aggregates that were more compact.

Moreover, the *C* constant calculated form BET equation showed substantial differences of the surface properties of the nanoparticles. This constant is proportional to $e^{(q1-qL)/RT}$, where q_1 is the heat of adsorption of the first layer, q_L the heat of liquefaction of the adsorptive, *R* the universal gas constant and *T* the absolute temperature. Consequently, it expresses the strength of the interaction between the adsorptive gas molecules and the surface. This strength was rather low for the organically coated surfaces, especially for the octylated one (~27). This is due to a practically complete covering of the SiO_2 surface with organic groups. However, concerning the uncoated inorganic surfaces, the *C* constant increased in the sequence SiO_2 – TiO_2 – ZnO, which is in agreement with the increasing density of these oxides.

Table 2. The properties of the nanoparticles used for cytotoxic testing.

Nanoparticles	Surface modification	S_{BET}*/ m² g⁻¹	C*	d* / nm
SiO_2	-	204	79	13
SiO_2–methyl	– CH_3	220	31	12
SiO_2–octyl	– $(CH_2)_7$ – CH_3	164	27	16
TiO_2	-	51	93	30
ZnO	-	46	139	23

*S_{BET}, BET surface area; *C*, constant of the BET equation; *d*, particle size calculated from the S_{BET} provided the crystals were approximated by a sphere.

In the cell culture medium, the nanoparticles exhibited a very good stability with an exception of the SiO_2 nanoparticles that formed clusters. Due to surface modification, the coated SiO_2 were more stable and no larger clusters were formed. Zeta potential of all the tested nanoparticles ranged from −14 to −20 mV. This indicates that the bovine serum albumin, the most abundant protein in serum (used as a dispersant), was adsorbed on the nanoparticle surface.

The difference of crystallinity between the nanoparticles was significant. While the semiconductor TiO_2 and ZnO nanoparticles exhibited a high degree of crystallinity, the SiO_2 coated and uncoated did not (Figure 2b). The pattern of TiO_2 P25 showed diffractions at 25.15° (101), 36.82° (103), 37.67° (004), 38.48° (112), 47.93° (200), 53.75° (105), and 54.96° (211) corresponding to the tetragonal anatase structure (space group I41/amd). Those at 27.33° (110), 35.93° (101), 41.18° (111), 54.21° (211), and 56.53° (220) are assigned to the tetragonal rutile structure (space group P42/mnm). From the diffractograms it follows that the proportion of anatase and rutile phases was approximately 4:1. The diffractions of ZnO matched those of hexagonal wurtzite structure (space group P63mc). Its pattern was characterized by the diffractions centered at 31.62° (100), 34.22° (002), 36.11° (101), 47.39° (102) and 56.47° (110). On the other hand, compared to highly crystalline TiO_2 and ZnO, the coated and uncoated SiO_2 nanoparticles showed amorphous character. The characteristic asymmetrical peak centered at ca. 22° indicates that in amorphous particles some small coherent regions were present.

FTIR spectra showed that the surface properties of the nanoparticles differed considerably (Figure 2c). All the tested nanoparticles exhibited a broad band ranging from 3200 to 3700 cm^{-1}, which corresponds to bridging H-bonded hydroxyls. This band is obviously overlapped with the sorbed water [19]. The peak centered at 3695 cm^{-1} belongs to free O–H vibrations [20], while the sharp peak at 3746 cm^{-1} represent "freely vibrating" surface hydroxyls in which each individual hydroxyl is sufficiently isolated to avoid interaction with neighboring hydroxyls. For the coated and uncoated SiO_2, the infrared group frequencies differed substantially. While SiO_2–octyl was characterized by stretching of alkyl –CH_3 (2964 and 2857 cm^{-1}) and –CH_2 (2928 cm^{-1}) bands, SiO_2–methyl represented only –CH_3 (2964 cm^{-1}) stretching vibrations. In the case of SiO_2, whose surface was not modified, these frequencies were not detected.

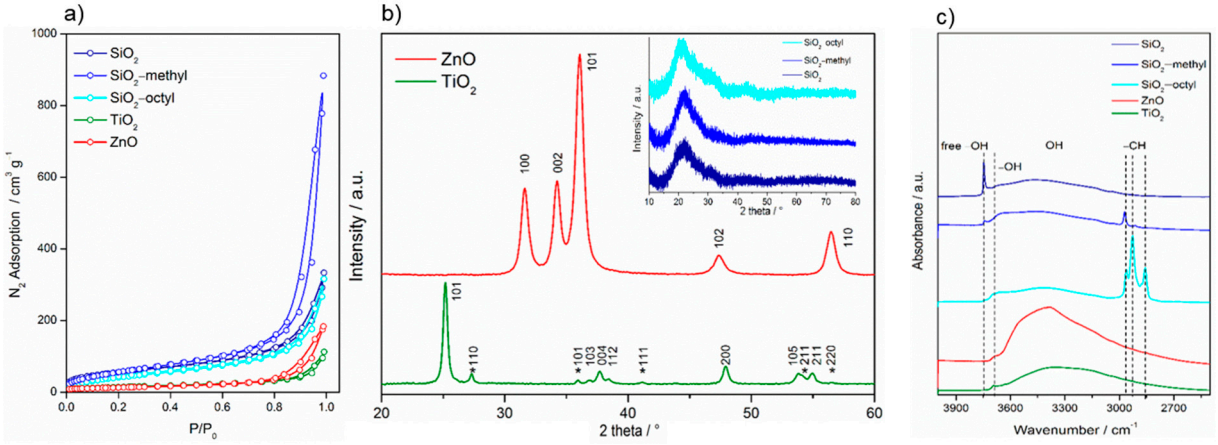

Figure 2. Nitrogen sorption isotherms of the nanoparticles determined at the boiling point of liquid nitrogen (a), XRD patterns of the nanoparticles (b), FTIR spectra of the nanoparticles (c).

3.2 Evaluation of the nanoparticles cytotoxicity

The evaluation of the WST-1 (cell metabolism) and LDH (cell integrity) assays showed that the cytotoxicity of the nanoparticles differed substantially. While the ZnO and SiO_2 nanoparticles exhibited statistically significant high toxicity towards the A549 human lung cells, no statistically significant cytotoxic effect was observed for the coated SiO_2 (–methyl, –octyl) and TiO_2 nanoparticles, up to their highest tested concentration of 250 μg L^{-1} (Figure 3). These results are in good agreement with the literature [21].

For the insoluble SiO_2 nanoparticles, the LC_{50} was roughly 90 μg mL^{-1} for both cytotoxic assays (Table 3). Generally, this observation is in good agreement with previous studies showing SiO_2 nanoparticles with induced cytotoxicity at concentrations of >25 μg mL^{-1} [22]. This can be explained by the formation of reactive oxygen species (ROS) inside the cells due to Si–OH surface groups [8] and/or by membrane damage mediated by hydrogen bonding [23].

On the other hand, for the insoluble coated SiO_2 (–octyl and –methyl) nanoparticles, no cytotoxicity towards the A549 cells was observed in both assays. It could be explained by the suppression of ROS formation due to the presence of surface functionalities that inhibit the reactivity of the Si–OH groups. Other reasons include the surface modifications influencing nanoparticle-membrane interactions, intracellular trafficking, inter-particle interactions, and/or dynamic changes to nanoparticle characteristics [24]. All these factors can affect cell viability.

Dose-dependent cytotoxicity was observed for the soluble ZnO nanoparticles, with LD_{50} being roughly 10 μg mL^{-1} for both assays. However, the cytotoxicity curve for the LDH assay was much less pronounced than the very sharp one for the WST-1 assay. This was probably due to the limited period for which the released LDH was present in the cell culture medium. After 24 h, the LDH enzyme may still be inside the cells whose programmed cell death terminates with membrane disruption. Alternatively, the LDH enzyme may have been degraded within the 24 h if cell death occurred shortly after exposure. The discrepancy between the results obtained using the LDH and WST-1 assays shows the importance of employing cytotoxicity assays with different endpoints to avoid underestimation of the results. Compared to the ZnO nanoparticles, the Zn^{2+} of $ZnCl_2$ had a considerably higher cytotoxic effect, with LD_{50} being roughly 5 μg L^{-1}. This is in agreement with the literature [25,26]. The lower cytotoxicity of the ZnO nanoparticles (8 μg L^{-1}) can be explained by the gradual release of zinc ions from the internalized nanoparticles as opposed to the complete dissolution of ZnCl2 in the cell culture. High concentrations of zinc ions can cause cell death by breakdown of the mitochondrial membrane potential [27].

For the insoluble TiO_2 nanoparticles, no statistically significant cytotoxicity was observed. This observation is in agreement with published data. For instance, after 48 h exposure in dark, no cytotoxicity was observed towards A549 lung cells up to a dose-concentration of 400 μg mL^{-1} [14].

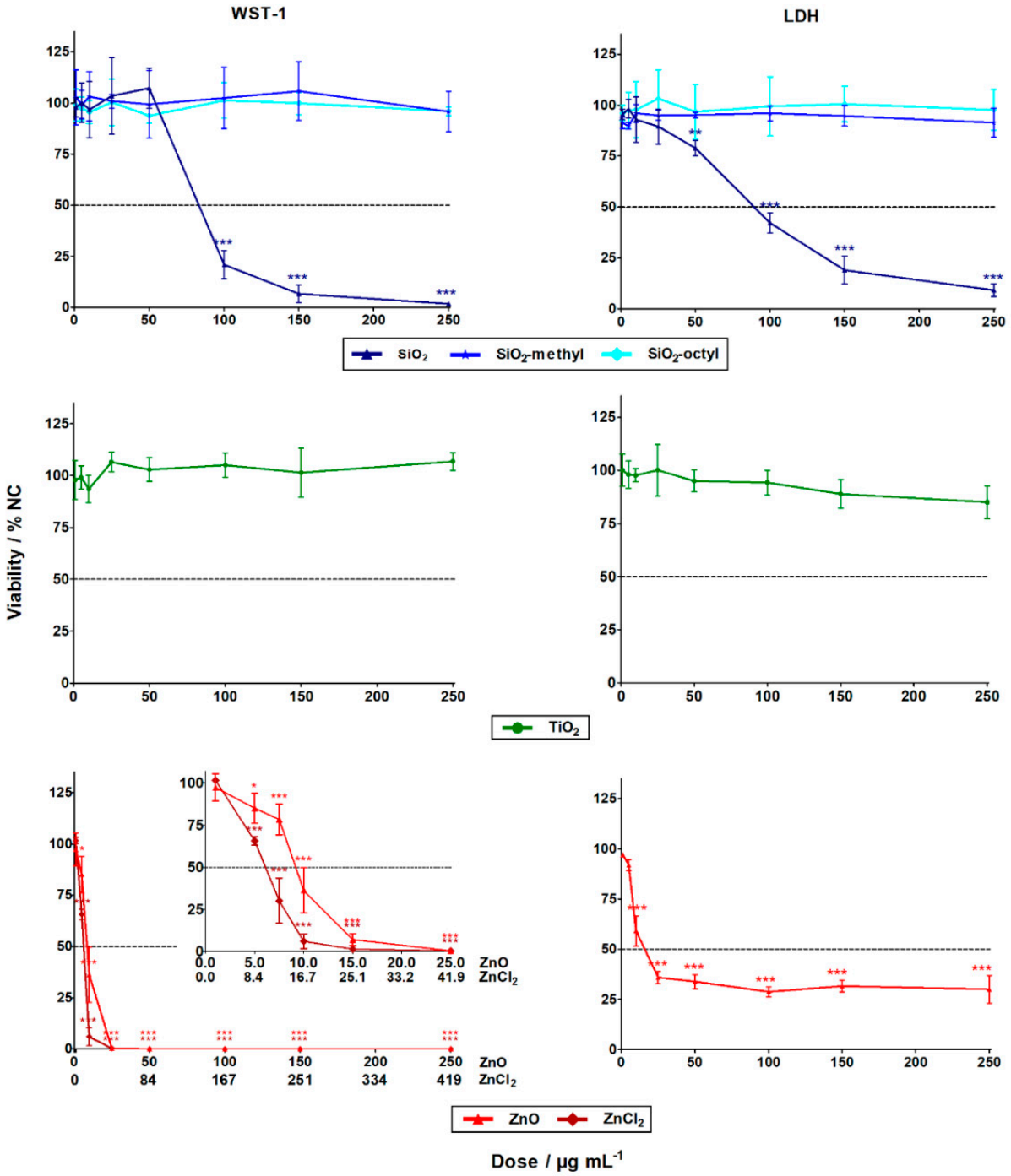

Figure 3. The cytotoxic effects of the nanoparticles and zinc salt ($ZnCl_2$) in A549 cells after 24 h exposure determined by WST-1 (left column) and LDH (right column) assays. The data points designated with stars were statistically significant, $p < 0.05$ (*), < 0.01 (**) and < 0.001 (***) compared to the negative control cells (NC).

Table 3 LC_{50} values obtained from both cytotoxic assays after 24 h exposure.

Sample	WST-1 assay / μg mL^{-1}	LDH assay / μg mL^{-1}
SiO_2	89.4 ± 1.2	92.0 ± 12.4
SiO_2–methyl	no toxic*	no toxic
SiO_2–octyl	no toxic	no toxic
TiO_2	no toxic	no toxic
ZnO	9.6 ± 0.2	9.5 ± 0.6
ZnO as Zn^{2+}	7.8 ± 0.2	7.7 ± 0.5
$ZnCl_2$	10.1 ± 0.6	NA
$ZnCl_2$ as Zn^{2+}	4.8 ± 0.3	NA

NA not available. *No toxic means that the particles did not exhibit cytotoxic effects at the test conditions.

3.3 Nanoparticles uptake by the lung cells

To better understand the cytotoxic test results, we employed transmission electron microscopy to investigate the localization of the nanoparticles within lung cells. The TEM analysis of ultrathin sections of the cells revealed considerable differences in the localization of the internalized nanoparticles (Figure 4).

For uncoated SiO_2, while a majority of the nanoparticles was observed in the cell cytoplasm, only small fraction of the nanoparticles was engulfed in the phagosomes. Along with intact phagosomes, partly disrupted ones were also observed, which presumably reflects nanoparticle release from phagosomes to cytoplasm. An increased production of autophagosomes engulfing nanoparticle-contaminated cytoplasm and organelles was observed. This increase can be due to the need to degrade the internalized nanoparticles and/or the disrupted parts of the cells. Owing to the presence of the nanoparticles in the cytoplasm, the formation of reactive oxygen species can be hypothesized as a mechanism of their toxicity.

SiO_2-octyl and SiO_2-methyl and TiO_2 nanoparticles were dominantly internalized inside the intact phagosomes as aggregates of various sizes. Their intact membrane isolating the nanoparticles from the internal cellular milieu protected the cells from potential toxic effect. No morphological changes of the cell ultrastructure were observed, which is in agreement with our toxicological results. Very rarely, a small portion of the nanoparticles were observed in the cytoplasm, however, this could be an artifact of the sectioning procedure.

For ZnO, virtually all of the cells were damaged displaying fragmented membranes and nuclei. An increased number of autophagosomes and lipid droplets was found. As no nanoparticles were observed either inside or outside the lung cells, we hypothesize that their intracellular dissolution to Zn^{2+} occurred. Velintine et al. (2017) observed the dissolution of ZnO nanoparticles already 1 hour after the cell exposure [28], which supports our hypothesis. Therefore, the cytotoxicity mechanism due to Zn^{2+} dissolved in the cytoplasm is plausible. However, we cannot exclude another mechanism due to nanoparticles themselves.

Peer-reviewed version available at Nanomaterials 2019, 9, 968; doi:10.3390/nano9070968

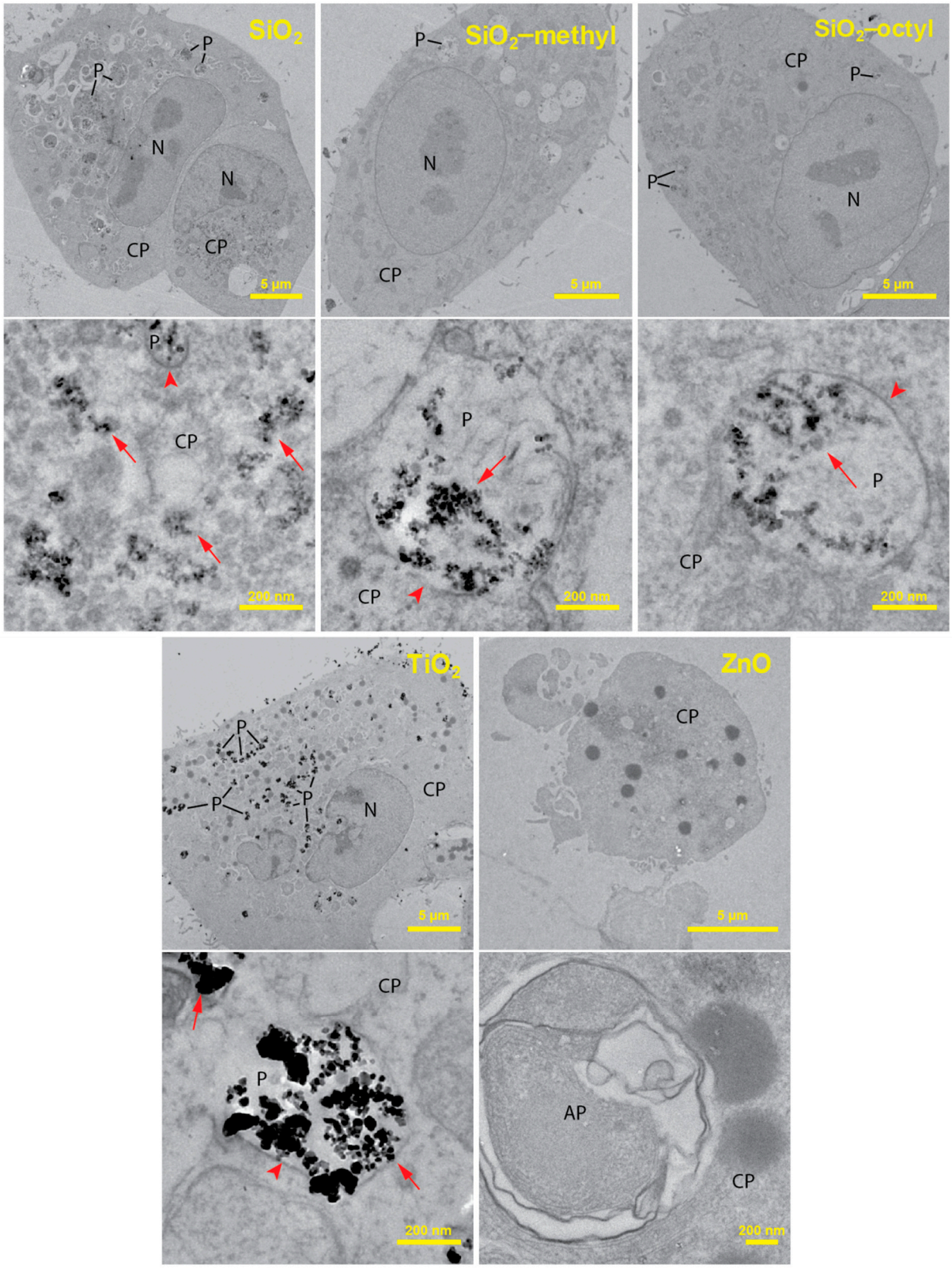

Figure 4. TEM cross-section images of the A549 cells after 24 h incubation with of TiO_2, ZnO, SiO_2 and modified SiO_2 nanoparticles at concentration of 10 µg mL^{-1}. For each nanoparticle type in the pair of images, the upper represents the whole cell while the lower its high magnification detail depicting intracellular localization of the nanoparticles in cytoplasm (CP) , phagosomes (P), autophagosomes (AP) and nuclei (N). Arrows indicate nanoparticles; arrowheads show phagosomal membranes around nanoparticles.

3.4 Improved strength of sandstone by nanoparticle-modified consolidants

The drilling resistance forces of the sandstone treated with various consolidants differed considerably. For instance, compared to the very low drilling resistance force for the reference sandstone (2 N), those for all the consolidated sandstone samples were much higher (Figure 5, Table 4). For the commercial consolidant KSE OH, the increase of the resistance was roughly three times (7 N). However, the highest drilling resistance forces were obtained for our novel nanoparticle-modified consolidants. The reason for the increase is most probably the improvement of the xerogel function properties [2,29]. They include the suppression of the gel cracking and shrinking inside the stone, the increase of the xerogel hardness due to the embedding of nanoparticles. Concerning the effect of various nanoparticles on the consolidant performance, the highest resistance force was achieved for the TiO_2 nanoparticles (26 N), while that of the ZnO nanoparticles was roughly about 14 N. The resistance for both coated and SiO_2 was in between those for TiO_2 and ZnO, ranging from ca. 17 to 22 N. Therefore, the SiO_2 nanoparticles can be replaced with coated ones without any loss of mechanical performance.

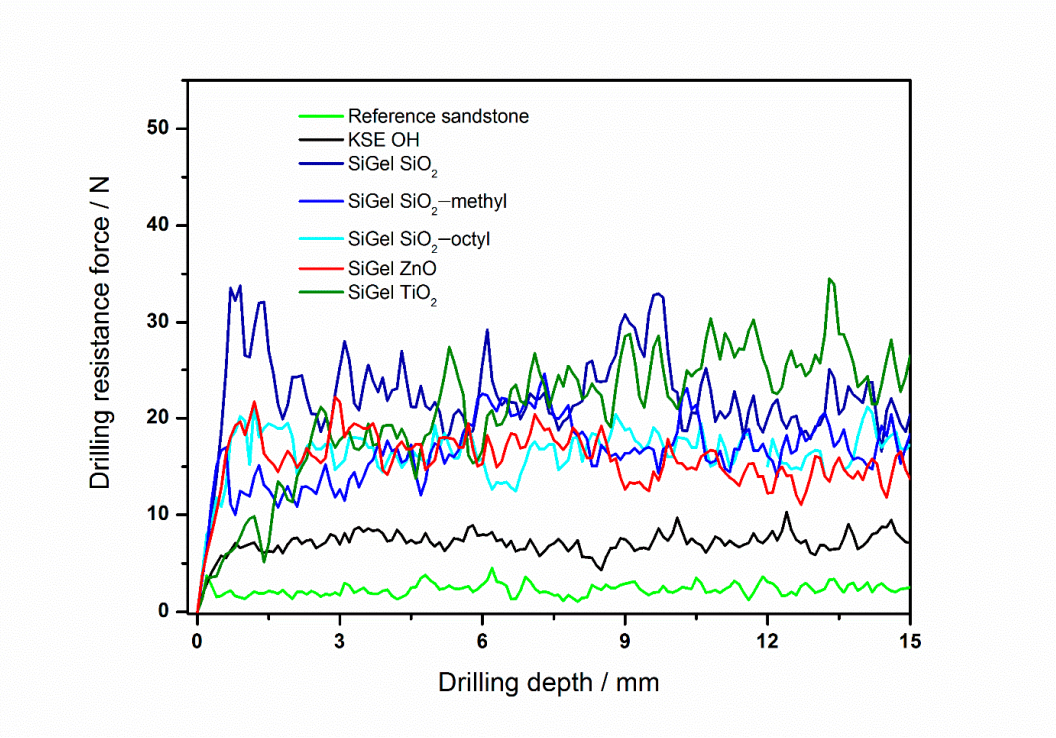

Figure 5. The drilling resistance profiles of reference sandstone and sandstones treated with various consolidants.

Table 4. Drilling resistance force for sandstone consolidated with various consolidants. The average values in the table were determined within the drilling depth from four to fourteen mm.

Consolidant	Drilling resistance force / N
Reference sandstone	2.4 ± 0.7
KSE OH	7.4 ± 1.2
SiGel SiO_2	22.3 ± 4.4
SiGel SiO_2-methyl	16.9 ± 3.3
SiGel SiO_2-octyl	17.3 ± 2.7
SiGel TiO_2	25.9 ± 6.8
SiGel ZnO	14.4 ± 2.9

4. Conclusions

Using two independent WST-1 and LDH assays, we have shown that the toxicity of various nanoparticles considerably differed. While the ZnO and SiO_2 exhibited substantial cytotoxic effects at the test conditions, the TiO_2 and both coated SiO_2 nanoparticles did not. TEM analysis of the cellular nanoparticle uptake helped to interpret the toxicological results. Due to the encapsulation of the TiO_2, SiO_2-octyl and SiO_2-methyl nanoparticles in the intact phagosomes, their effects on cell viability was minimalized. However, the presence of the SiO_2 nanoparticles in the cell cytoplasm caused their cytotoxicity. On the other hand, the cytotoxicity of the ZnO nanoparticles was probably caused by their dissolution at the acidic conditions inside the phagosomes. Compared to sandstone and sandstone treated with commercial consolidant, our novel nanoparticle-modified consolidants increased the stone strength by ten- and three-times, respectively. Our research showed that the often-used toxic nanoparticles (SiO_2, ZnO) can be replaced by non-toxic equivalents (coated SiO_2, TiO_2) without any performance impairment. Thus, the combination of a toxicological study and materials research enabled to formulate novel consolidants, which not only overcome the performance of commonly used ones but also are safer for human health and the environment.

Author Contributions: conceptualization, Jiri Rathousky; methodology, Monika Remzova and Jan Topinka; validation, Tana Brzicova and Pavel Rossner; formal analysis, Pavel Rossner; investigation, Monika Remzova, Radek Zouzelka and Kristyna Vrbova; data curation, Tana Brzicova; writing—original draft preparation, Radek Zouzelka; writing—review and editing, Jiri Rathousky; supervision, Jan Topinka; project administration, Jan Topinka and Jiri Rathousky.

Funding: This research was funded by the Czech Science Foundation, grant number 17-18972S.

Acknowledgments: The study was further supported by the Ministry of Education, Youth and Sports of the Czech Republic, project number LO1508. The authors acknowledge the assistance provided by the Research Infrastructures NanoEnviCz (Project No. LM2015073) supported by the Ministry of Education, Youth and Sports of the Czech Republic and the project Pro-NanoEnviCz (Reg. No. CZ.02.1.01/0.0/0.0/16_013/0001821) supported by the Ministry of Education , Youth and Sports of the Czech Republic and the European Union - European Structural and Investments Funds in the frame of Operational Programme Research Development and Education. The HRTEM experiments were supported by the Czech-BioImaging large RI project (LM2015062 funded by MEYS CR) and by OP RDE (CZ.02.1.01/0.0/0.0/16_013/0001775 "Modernization and support of research activities of the national infrastructure for biological and medical imaging Czech-BioImaging").

Conflicts of Interest: The authors declare no conflict of interest. The funders had no role in the design of the study; in the collection, analyses, or interpretation of data; in the writing of the manuscript, or in the decision to publish the results.

References

1. Hornyak, G., Tibbals, H., Dutta, J., Moore, J. *Introduction to Nanoscience and Nanotechnology*; 1st Editio.; 2008; ISBN 9781420047806.

2. Miliani, C.; Velo-Simpson, M.L.; Scherer, G.W. Particle-modified consolidants: A study on the effect of particles on sol-gel properties and consolidation effectiveness. *J. Cult. Herit.* **2007**, *8*, 1–6.

3. Kislov, N.; Lahiri, J.; Verma, H.; Goswami, D.Y.; Stefanakos, E.; Batzill, M. Photocatalytic degradation of methyl orange over single crystalline ZnO: Orientation dependence of photoactivity and photostability of ZnO. **2009**, 3310–3315.

4. Guérin, V.-M.; Zouzelka, R.; Bibova-Lipsova, H.; Jirkovsky, J.; Rathousky, J.; Pauporté, T. Experimental and DFT study of the degradation of 4-chlorophenol on hierarchical

micro-/nanostructured oxide films. *Appl. Catal. B Environ.* **2015**, *168–169*, 132–140.

5. Zouzelka, R.; Kusumawati, Y.; Remzova, M.; Rathousky, J.; Pauporte, T. Photocatalytic activity of porous multiwalled carbon nanotube-TiO_2 composite layers for pollutant degradation. *J. Hazard. Mater.* **2016**, *317*, 52–59.

6. Zouzelka, R.; Rathousky, J. Photocatalytic abatement of NOx pollutants in the air using commercial functional coating with porous morphology. *Appl. Catal. B Environ.* **2017**, *217*, 466–476.

7. Zouzelka, R.; Remzova, M.; Brabec, L.; Rathousky, J. Photocatalytic performance of porous TiO_2 layers prepared by quantitative electrophoretic deposition from organic solvents. *Appl. Catal. B Environ.* **2018**, *227*, 70–78.

8. Li, Y.; Yu, Y.; Sun, Z.; Duan, J.; Tian, L.; Ho, K.; Zhou, X.; Liu, X.; Yu, Y. Silica nanoparticles induce autophagy and autophagic cell death in HepG2 cells triggered by reactive oxygen species. *J. Hazard. Mater.* **2014**, *270*, 176–186.

9. Xu, Y.; Wang, N.; Yu, Y.; Li, Y.; Li, Y.B.; Yu, Y.B.; Zhou, X.Q.; Sun, Z.W. Exposure to Silica Nanoparticles Causes Reversible Damage of the Spermatogenic Process in Mice. *PLoS One* **2014**, *9*, 1–11.

10. Nemmar, A.; Beegam, S.; Yuvaraju, P.; Yasin, J.; Attoub, S.; Ali, B.; Albarwani, S. Amorphous silica nanoparticles impair vascular homeostasis and induce systemic inflammation. *Int. J. Nanomedicine* **2014**, *9*, 2779.

11. Stark, W.J. Nanoparticles in biological systems. *Angew. Chemie - Int. Ed.* **2011**, *50*, 1242–1258.

12. Krug, H.F.; Wick, P. Nanotoxicology: An interdisciplinary challenge. *Angew. Chemie - Int. Ed.* **2011**, *50*, 1260–1278.

13. Guo, D.; Wu, C.; Jiang, H.; Li, Q.; Wang, X.; Chen, B. Synergistic cytotoxic effect of different sized ZnO nanoparticles and daunorubicin against leukemia cancer cells under UV irradiation. *J. Photochem. Photobiol. B Biol.* **2008**, *93*, 119–126.

14. Ekstrand-Hammarström, B.; Akfur, C.M.; Andersson, P.O.; Lejon, C.; Österlund, L.; Bucht, A. Human primary bronchial epithelial cells respond differently to titanium dioxide nanoparticles than the lung epithelial cell lines A549 and BEAS-2B. *Nanotoxicology* **2012**, *6*, 623–634.

15. Clemente, Z.; Castro, V.L.S.S.; Moura, M.A.M.; Jonsson, C.M.; Fraceto, L.F. Toxicity assessment of TiO_2 nanoparticles in zebrafish embryos under different exposure conditions. *Aquat. Toxicol.* **2014**, *147*, 129–139.

16. Zouzelka, R.; Cihakova, P.; Rihova Ambrozova, J.; Rathousky, J. Combined biocidal action of silver nanoparticles and ions against Chlorococcales (Scenedesmus quadricauda, Chlorella vulgaris) and filamentous algae (Klebsormidium sp.). *Environ. Sci. Pollut. Res.* **2016**, *23*, 8317–

422 8326.

423 17. Ohtani, B.; Li, D.; Abe, R. What is Degussa (Evonik) P25 ? Crystalline composition analysis ,
424 reconstruction from isolated pure particles and photocatalytic activity test. *J. Photochem.*
425 *Photobiol. A Chem.* **2010**, *216*, 179–182.

426 18. Ritz, C.; Streibig, J.C. Bioassay Analysis using R . *J. Stat. Softw.* **2015**, *12*.

427 19. Li, L.; Yan, J.; Wang, T.; Zhao, Z.-J.; Zhang, J.; Gong, J.; Guan, N. Sub-10 nm rutile titanium
428 dioxide nanoparticles for efficient visible-light-driven photocatalytic hydrogen production.
429 *Nat. Commun.* **2015**, *6*, 5881.

430 20. Arrouvel, C.; Digne, M.; Breysse, M.; Toulhoat, H.; Raybaud, P. Effects of morphology on
431 surface hydroxyl concentration: A DFT comparison of anatase-TiO_2 and γ-alumina catalytic
432 supports. *J. Catal.* **2004**, *222*, 152–166.

433 21. Tedesco, E.; Mičetić, I.; Micheletti, C.; Ciappellano, S.G.; Benetti, F.; Venturini, M.
434 Cytotoxicity and antibacterial activity of a new generation of nanoparticle-based
435 consolidants for restoration and contribution to the safe-by-design implementation. *Toxicol.*
436 *Vitr.* **2015**, *29*, 1736–1744.

437 22. Lison, D.; Martens, J.A.; Hoet, P.H.; Napierska, D.; Thomassen, L.C. The nanosilica hazard:
438 another variable entity. *Part. Fibre Toxicol.* **2010**, *7*, 39.

439 23. Fruijtier-Pölloth, C. The toxicological mode of action and the safety of synthetic amorphous
440 silica-A nanostructured material. *Toxicology* **2012**, *294*, 61–79.

441 24. Oh, W.; Kim, S.; Choi, M.; Kim, C.; Jeong, Y.S.; Cho, B.; Hahn, J.; Jang, J. Cellular uptake,
442 cytotoxicity, and innate immune response of silica− titania hollow nanoparticles based on
443 size and surface functionality. *ACS Nano* **2010**, *4*, 5301–5313.

444 25. Cho, W.S.; Duffin, R.; Howie, S.E.M.; Scotton, C.J.; Wallace, W.A.H.; MacNee, W.; Bradley,
445 M.; Megson, I.L.; Donaldson, K. Progressive severe lung injury by zinc oxide nanoparticles;
446 the role of Zn2+dissolution inside lysosomes. *Part. Fibre Toxicol.* **2011**, *8*, 27.

447 26. Amara, S.; Slama, I. Ben; Mrad, I.; Rihane, N.; Khemissi, W.; El Mir, L.; Rhouma, K. Ben;
448 Abdelmelek, H.; Sakly, M. Effects of zinc oxide nanoparticles and/or zinc chloride on
449 biochemical parameters and mineral levels in rat liver and kidney. *Hum. Exp. Toxicol.* **2014**,
450 *33*, 1150–1157.

451 27. Wätjen, W.; Haase, H.; Biagioli, M.; Beyersmann, D. Induction of apoptosis in mammalian
452 cells by cadmium and zinc. *Environ. Health Perspect.* **2002**, *110*, 865–867.

453 28. Velintine, V.A.; Wee, B.S.; Chin, S.F.; Kok, K.Y. Transformation of zinc oxide nanoparticles
454 under environmentally relevant conditions: influence of pH and ionic strength. *Trans. Sci.*
455 *Technol.* **2017**, *4*, 123–136.

29. Remzova, M.; Sasek, P.; Frankeova, D.; Slizkova, Z.; Rathousky, J. Effect of modified ethylsilicate consolidants on the mechanical properties of sandstone. *Constr. Build. Mater.* **2016**, *112*, 674–681.